



# City Research Online

## City, University of London Institutional Repository

---

**Citation:** Le, B., Goodey, R.J. and Divall, S. ORCID: 0000-0001-9212-5115 (2019). Subsurface ground movements due to circular shaft construction. *Soils and Foundations*, doi: 10.1016/j.sandf.2019.03.013

This is the accepted version of the paper.

This version of the publication may differ from the final published version.

---

**Permanent repository link:** <https://openaccess.city.ac.uk/id/eprint/21932/>

**Link to published version:** <http://dx.doi.org/10.1016/j.sandf.2019.03.013>

**Copyright and reuse:** City Research Online aims to make research outputs of City, University of London available to a wider audience. Copyright and Moral Rights remain with the author(s) and/or copyright holders. URLs from City Research Online may be freely distributed and linked to.

---

City Research Online:

<http://openaccess.city.ac.uk/>

[publications@city.ac.uk](mailto:publications@city.ac.uk)

---

## **Subsurface ground movements due to circular shaft construction**

### **Abstract**

The rapid development of modern metropolises has led to a shortage of surface space and in response engineers have pursued alternatives below ground level. Shafts are commonly used to provide temporary access to the subsurface for tunnelling and, as permanent works, are utilised for lifts or ventilation purposes. The construction sequence of axisymmetric shafts makes them a dramatically simple solution. In addition, circular shafts are inherently stiffer than other plan geometries. Those, perhaps, are reasons why circular shafts are preferred in situations of restricted space or unfavourable ground conditions. However, due to the lack of case histories reporting ground movements induced by shaft construction, no empirical prediction method for subsurface soil displacements exists. The work presented here seeks to provide clearer insights into surface and subsurface soil displacements induced by circular shaft construction by means of analysis on measurements obtained from centrifuge tests and available field data. Novel empirical equations and procedures are suggested for practical use.

### **Keywords**

Shaft construction; Ground movements; Centrifuge modelling

## LIST OF SYMBOLS

$a$	Constant indicates the depth at which maximum horizontal displacement occurs
$b$	Constant governs the height of the Gaussian curve
$d$	Distance from shaft wall
$D$	Shaft diameter
$H$	Shaft depth
$K_0$	Ratio between horizontal and vertical effective stresses at rest
OCR	Overconsolidation ratio
$n$	Multiple of shaft depth, $H$ , to a distance $d$ from the shaft wall where settlement becomes zero
$S$	Soil displacement
$S_v$	Vertical soil displacement
$S_h$	Horizontal soil displacement
$S_v^{dz}$	Vertical displacement at depth $z$ and at a distance $d$ from shaft wall
$S_h^{dz}$	Horizontal displacement at depth $z$ and at a distance $d$ from shaft wall
$S_u$	Undrained shear strength of clay
$\alpha$	Empirical constant
$\phi'_c$	Critical state angle of shearing resistance
$\sigma'_h$	Horizontal effective stress
$\sigma'_v$	Vertical effective stress
$\sigma'_{v0}$	Maximum consolidation pressure for clay model in centrifuge test

1 INTRODUCTION

2

3 In urban environments shafts are often, by necessity, constructed adjacent to existing  
4 underground structures such as tunnels, deep foundations and basements. This makes the  
5 understanding of subsurface ground deformations and how they relate to surface displacement  
6 profiles increasingly important in assessing the possible effects of shaft excavation on nearby  
7 structures.

8

9 Faustin (2017) found that the magnitude and extent of ground deformations depends greatly on  
10 the shaft construction technique which can be classified by two categories: pre-installed shaft  
11 lining and concurrent shaft lining. In the former category, the shaft lining is installed before the  
12 shaft is excavated. The shaft lining can be formed by precast lining, diaphragm wall or sheet  
13 piles. The concurrent shaft lining involves excavation and then construction of the shaft lining. In  
14 concurrent shaft lining methods, spray-concrete lining (SCL) or precast segments are often  
15 used to form the lining.

16

17 The sources of ground deformations induced by shaft construction are depicted in **Figure 1**  
18 (after Faustin, 2017) and described below;

19 i) Radial unloading:

- 20 - For concurrent shaft construction: removing soil causes stress relief that results in soil  
21 movements into the shaft cavity before the lining is installed.
- 22 - For pre-installed shaft lining: when soil within the lining is removed, the unbalanced  
23 horizontal stresses are transferred to the shaft lining resulting in lining compression,  
24 leading to horizontal and vertical soil displacements. As the soil is supported by the  
25 shaft lining, the magnitude of soil displacements is expected to be smaller than that in  
26 concurrent shaft construction where the horizontal stress was reduced to zero without  
27 support prior to the shaft lining being installed. This was confirmed by back analysis on  
28 field data reported by Faustin (2017).

29 ii) Vertical unloading of the excavated base causes heave at the shaft plug which also  
30 contributes to the total soil deformation.

31 iii) Changes in the ground water table due to dewatering causes settlement. However,  
 32 dewatering is not necessarily performed in all cases.

33 iv) Consolidation due to the changes in pore water pressure in the ground re-establishing  
 34 equilibrium as a result of the excavation process. In the available case histories, only Schwamb  
 35 (2014) reported long-term settlements which were considered minor compared with those which  
 36 occurred during diaphragm wall construction. Because of this lack of reliable long term data, the  
 37 current work only reports and analyses short-term soil displacements due to shaft excavation  
 38 and does not consider long-term movements due to either consolidation or creep.

39

40 Up to 2016 there have been only a few empirical approaches for surface settlement  $S_v^{surface}$   
 41 prediction including the widely used equation suggested by New & Bowers (1994).

$$S_v^{surface} = \alpha H \left(1 - \frac{d}{H}\right)^2 \quad (1)$$

42

43 It is important to note that **Equation 1** was derived from field measurements from only one shaft  
 44 with  $H = 26m$  and  $D = 11m$ , constructed using the concurrent shaft sinking technique in London  
 45 Clay. Prediction of surface settlements using this equation would be dependent on the adopted  
 46 value of  $\alpha$ . In the original work, the reported value of  $\alpha = 6 \times 10^{-4}$  provided the best fit with the  
 47 field data presented in New & Bowers (1994) but the literature does not contain any further  
 48 reported values (Schwamb et al., 2016). **Equation 1** is acknowledged to be quite conservative,  
 49 particularly for pre-installed shafts (Schwamb, 2014; Faustin, 2017) because, for those  
 50 conditions, the settlements are expected to be smaller as discussed earlier.

51

52 New (2017) studied field data from 13 shaft construction projects, with diameter range of  $D =$   
 53  $6.5$  to  $16.6m$ , and found that the magnitude of surface settlement increases with larger shaft  
 54 diameter (**Figure 2**). An extension to New & Bowers (1994) original equation was suggested by  
 55 New (2017) which introduces a new variable,  $n$ , which governs that the surface settlement  
 56 becomes zero at a distance of  $nH$  from the shaft wall, as described in **Equation 2**;

$$S_v^{surface} = \alpha H \left(1 - \frac{d}{nH}\right)^2 \quad (2)$$

57 The field measurements presented by New (2017) are all from projects in stiff London Clay with  
58 a similar construction technique. As such, the original value of  $\alpha$  was retained in this work but  
59 values of  $n$  and  $\alpha$  would be expected to increase in softer soils. New (2017) suggested that  
60 designers can consider **Equation 2** as a predictive tool with the values of  $n$  and  $\alpha$  to be chosen  
61 dependent on the required degree of conservatism and that they should be supported by field  
62 data from similar shaft projects. New (2017) also acknowledged that surface settlement  
63 predictions are varied and difficult to make due to a lack of available field data. Whilst this work  
64 enables designers to assess surface settlements, there is no empirical approach to predict  
65 subsurface soil displacements even though more shafts are being constructed in crowded and  
66 sensitive urban areas with existing buried structures. These structures may require assessment  
67 of the effect of adjacent shaft construction in order that their serviceability is maintained.

68

69 The main purpose of the study presented in this paper is to gain a better insight into subsurface  
70 soil displacements induced by shaft construction by the means of centrifuge modelling and back  
71 analysis on available case histories.

72

### 73 CASE STUDIES

74 An extensive literature review on shaft construction, carried out by Faustin (2017), shows that  
75 there have been only 18 case histories on circular shaft construction published between 1980  
76 and 2016. There have been some additional cases in 2017 (Faustin, 2017; New, 2017). Most of  
77 these case studies report surface settlement, only 3 cases presenting subsurface soil  
78 displacements and only 1 case reported surface horizontal displacement. Details of case  
79 histories used in this section are presented in **Table 1** with shaft geometries, construction  
80 techniques and soil conditions included.

81

82 It is worth noting that not all measurements from these publications are reported in this paper.  
83 Even though there were data from four extensometers in Schwamb et al. (2016), the readings  
84 from two of them were less than 0.5mm which is well below the resolution of the instrumentation  
85 and are therefore not presented here. Hence only readings from two extensometers in Wong &

86 Kaiser (1988) and Schwamb et al. (2016) are used for subsurface vertical displacements  
87 analysis.  
88  
89 Only one in two inclinometer measurements reported by McNamara et al. (2008) and Wong &  
90 Kaiser (1988) are also utilised in this study. This is because the other inclinometer readings  
91 were either affected by existing piles (McNamara et al., 2008) or not fully reported; possibly due  
92 to poor accuracy (Wong & Kaiser, 1988) and hence these are not used.

93  
94 Even though there were two data sets for horizontal and vertical surface displacements  
95 available in New & Bowers (1994), only one set was used because the other was deemed  
96 unreliable due to the effects of heavy plant movements and nearby excavations.

97  
98 The rarity of high quality field measurements from shaft construction in the literature is possibly  
99 due to the high cost of monitoring schemes especially for deep shaft construction where deep  
100 drilling, for casings to house inclinometers and extensometers, is required to be below the shaft  
101 plug level in order to achieve representative results. In addition, shaft construction sites are  
102 normally occupied with activities that may affect the measurements leading to unrepresentative  
103 data and the existence of the underground structures that may alter the soil deformation  
104 mechanisms which causes difficulties in the interpretation of the measurement results.

105  
106 The challenges in obtaining representative soil displacements due to shaft construction can be  
107 overcome by the centrifuge modelling technique due to its advantageous capabilities in  
108 modelling soil behaviour in geotechnical events (Taylor, 1995). Recent developments in  
109 technology allows accurate measurement of soil deformations at any position in small scale  
110 centrifuge models (Stanier et al., 2015; Le et al., 2016).

111

## 112 CENTRIFUGE TESTING

113 A bespoke centrifuge model (**Figure 3**) was designed and used to investigate soil deformations  
114 induced by shaft construction and is described here.

115

116 *Test series*

117 The tests were performed using a fixed geometry but varying undrained shear strength  $S_u$  of the  
118 clay. The clay model (Speswhite kaolin) was one dimensionally consolidated in a soil container  
119 (known as a strong box) using a hydraulic consolidometer to a maximum vertical effective stress  
120  $\sigma'_{v0}$  equal to  $350kPa$  and  $500kPa$  for test CR350 and CR500, respectively. The samples were  
121 swelled back to a vertical stress of  $250kPa$  for both tests. The consolidation pressures were  
122 chosen for three reasons:

- 123 - To achieve overconsolidated soils, representative of real soil in urban environments  
124 (Parry, 1970);
- 125 - For the clay to be stiff enough for model making;
- 126 - For the clay not to be so stiff such that the soil deformations, induced by the simulated  
127 shaft excavation, would not be too small to measure accurately.

128

129 The water table was set at soil surface level. Properties of the Speswhite kaolin used can be  
130 found in Grant (1998). More details on the testing apparatus and procedure can be found in  
131 Divall & Goodey (2016) and are described briefly below.

132

133 *Test apparatus*

134 A schematic of the centrifuge model is illustrated in **Figure 3**. The excavation was simulated by  
135 a semi-circular cavity cut into the clay which could be viewed through the front Perspex window  
136 of the centrifuge model container. The dimensions of the excavation are  $D = 80mm$  and  $H =$   
137  $200mm$ . The excavation is supported by two components:

- 138 - The shaft liner (**Figure 3b**):  $200mm$  high,  $71mm$  in diameter. The cavity in the shaft plug  
139 (**Figure 3b**) has an internal diameter of  $65mm$  and  $45mm$  deep to allow basal heave to  
140 develop during the excavation simulation.
- 141 - A latex bag encloses the shaft liner with the cavity filled with a heavy fluid (commercially  
142 known as Sodium Polytungstate or SPT). This SPT fluid was prepared to have a density  
143 equal to the clay used in the model,  $17.5kN/m^3$ , to provide support to the soil.

144



145 The latex bag has a thickness of 1.5mm and together with the liner with radius of  $R$  equal to  
146 35.5mm leaves a void of 3mm between the excavation and the liner. This is initially supported  
147 by the heavy fluid of which the head was set to be level with the ground surface. The  
148 excavation process was simulated by draining the heavy fluid to generate radial and vertical  
149 unloading that results in ground deformations including heaving at the bottom of the shaft.

150

151 It is worth noting that using heavy fluid to support the soil implies an assumption that  $K_0 = 1$ , i.e.  
152  $\sigma'_v = \sigma'_h$ , within the soil mass which is slightly different from the  $K_0$  calculated by **Equation 3**  
153 (Mayne & Kullhawy, 1982) and shown in **Figure 4**.

$$K_0 = (1 - \sin\phi'_c)OCR^{sin\phi'_c} \quad (3)$$

154 For Speswhite kaolin,  $\phi'_c = 23^\circ$  (Grant, 1988). It can be seen that  $K_0$  values calculated by  
155 **Equation 3** for the soil along the shaft depth (0 to 200mm) are close to 1 (**Figure 4**). Near the  
156 surface the values of  $K_0$  are much larger. However, as the vertical stresses near the surface are  
157 very small the effect of this dissimilarity in  $K_0$  is negligible and was confirmed by good  
158 agreement between the centrifuge test results and field measurements which are presented  
159 later in this paper.

160

#### 161 *Test procedure*

162 On the test day, the strong box was removed from the hydraulic consolidometer to begin the  
163 model making procedure. All exposed surfaces of the clay sample were sealed with silicone oil  
164 to prevent drying and from this point onwards the model making process was carried out as  
165 rapidly as possible in order to preserve the stress history of the soil. The clay was then trimmed  
166 to the correct model height and the semi-circular cavity was cut for the shaft support system to  
167 be placed within. The front face of the clay model was sprayed with dyed Leighton Buzzard  
168 Sand (fraction B) to create the texture necessary for optimising the geoPIV post-test analysis.  
169 The front Perspex window was then bolted to the model container before the heavy fluid was  
170 injected into the rubber bag.

171

172 The models were accelerated to 100g and left running until the clay had reached effective stress  
173 equilibrium. The excavation process was then simulated by draining the heavy fluid. Data  
174 relating to deformations of the clay model and heavy fluid level were recorded at 1 second  
175 intervals for later analysis. In practice, the unloading rate varies in different projects due to  
176 different soil conditions, shaft geometries, and construction techniques. Therefore, the  
177 construction rate for these centrifuge tests was selected to ensure an undrained response to  
178 unloading. The total time required to simulate the complete unloading event was 25s in the  
179 centrifuge which represents around 2.5 days at prototype scale. The model was then spun down  
180 and shear vane readings were carried out to determine undrained shear strength,  $S_u$ , of the clay  
181 model. The average  $S_u$  of the model clay from surface to the shaft plug were 44.5kPa and  
182 57.8kPa for tests CR350 and CR500, respectively.

183

#### 184 *Measurement of soil movements*

185 GeoPIV\_RG (Stanier *et al.*, 2015) was used to analyse soil movements at the front face of the  
186 model from digital images taken during the test (**Figure 3a**). One of the drawbacks of the use of  
187 digital image analysis in centrifuge modelling is the friction at the interface between the Perspex  
188 window and the soil model that may affect the soil movement mechanism. However, results  
189 from image analysis reported by Grant (1998), Divall (2013) and Le (2017) showed that once  
190 the soil at the interface moved, it continued to displace at the same rate as the rest of the  
191 model. Therefore, the friction at the interface is negligible to the development of soil  
192 displacements and its mechanisms. Le (2017) conducted a series of shear box tests to examine  
193 the friction at the interface and found that the texture material was the key factor. In this  
194 research Leighton Buzzard Sand was used as it induced less friction compared with other  
195 texture material (e.g. glass balotini) owing to its lower angle of friction.

196

#### 197 TEST RESULTS

198 Typical soil displacements, immediately after the all of the fluid was drained out of the rubber  
199 bag, in the centrifuge test CR500 are presented in **Figure 5a** and the corresponding  
200 displacement contours are presented in **Figure 5b**. It can be seen that soil displacement is  
201 symmetrical (**Figure 5a**). From **Figure 5b**, soil displacements in the vertical and horizontal

202 directions become very small (less than 0.01mm) at a distance of 150 to 200mm from the shaft  
203 centreline. This confirms that the soil container was large enough and boundary effects were  
204 negligible.

205

206 **Figure 6** illustrates vertical and horizontal soil displacements in test CR500 at various distances  
207 up to 80mm ( $0.4H$ ) away from the shaft wall. For clarity, only data on one side of the model is  
208 presented. Vertical displacement increases towards the shaft wall and decreases with depth  
209 which is similar to observations made by previous researchers (New & Bowers, 1994; New,  
210 2017; Faustine, 2017; Schwamb et al., 2016). Interestingly, the profile of displacements,  $S_h$  and  
211  $S_v$ , with depth,  $z$ , at various distances from the shaft wall (up to  $d = 40\text{mm} = 0.2H$ ), show similar  
212 distribution patterns. For data at a distance beyond 40mm from the shaft wall, for example  $d =$   
213 80mm (**Figure 6**), the distribution of displacement with depth shows a different shape. Further  
214 analysis on subsurface and surface soil displacements is discussed below.

215

216 *Subsurface soil vertical displacements*

217 **Figure 7** presents subsurface vertical movement profiles at various distances  $d = 0.05H$  to  $0.2H$   
218 from the shaft wall at the end of the two centrifuge tests along with data from Wong & Kaiser  
219 (1988) and Schwamb et al. (2016). Vertical movement at depth  $z$  and a distance  $d$  from the wall,  
220  $S_v^{dz}$ , is normalised by maximum settlement at that distance,  $S_{vmax}^d$ , and  $z$  is normalised by  $H$ .  
221 The results from both centrifuge tests fit well with data from Wong & Kaiser (1988) but not with  
222 data from Schwamb et al. (2016) and the likely reason is explained below.

223

224 In Schwamb et al. (2016), the extensometer readings were baselined with bottom anchors  
225 which were installed at depths higher than that of the base of the shaft. The extensometer  
226 readings can only reflect absolute movements if the bottom anchors are fixed. However, finite  
227 element analysis showed that removal of the overburden pressure at excavation surface caused  
228 the adjacent ground to heave and the bottom anchor of the rod extensometers to move upwards  
229 by approximately 3mm (Schwamb et al., 2016). The heave behaviour near the shaft plug is  
230 confirmed by the centrifuge tests (**Figures 5, 6 & 7**). If the extensometer data are corrected by  
231 adding 3mm to the readings then the profile of subsurface vertical movements from Schwamb et

232 al. (2016) (labelled as corrected) are also in good agreement with other data (**Figure 7**). It is  
 233 worth noting that the bottom extensometer in Wong & Kaiser (1988) was installed into clay shale  
 234 layer, presumably a very stable stratum, and below the shaft plug level.

235

236 Despite the differences in soil conditions, construction techniques and excavation dimensions in  
 237 the considered shafts, vertical movements at depth  $z$ ,  $S_v^z$ , when plotted in the manner of **Figure**  
 238 **7**, show a consistent distribution which can be described by **Equation 4**;

$$\frac{S_v^{dz}}{S_{vmax}^d} = 1.15 - \frac{0.15}{1 - z/H} \quad (4)$$

(applicable for  $z \leq 0.9H$ )

239

240 **Equation 4** and **Figure 7** show that maximum vertical movement occurs near the ground  
 241 surface (when  $z = 0$ ) and decreases with depth.

242

243 *Subsurface soil horizontal displacements*

244 **Figure 8** presents subsurface horizontal soil movements in the considered shafts, reported by  
 245 McNamara et al. (2008) and Wong & Kaiser (1988), together with results from two centrifuge  
 246 tests. Horizontal movement at depth  $z$  and at a distance  $d$  from the wall,  $S_h^{dz}$ , is normalised  
 247 against the maximum horizontal displacement at that radial distance,  $S_{hmax}^d$  and the depth  $z$  is  
 248 normalised against  $H$ . Despite there being some anomalies from field measurements, most of  
 249 the data points agree well with the trend shown by the centrifuge test results.

250

251 The profile of horizontal soil movement with depth shows a similar distribution to a Gaussian  
 252 curve with the maximum value at  $z/H = 0.6$  to  $0.8$ . This is thought to be analogous to the  
 253 horizontal load distribution against a retaining wall where the load acts at depth  $z/H = 2/3 \approx$   
 254  $0.67$ . A best fit Gaussian curve (**Equation 5**) is proposed and also plotted in **Figure 8**.

$$\frac{S_h^{dz}}{S_{hmax}^d} = \exp \left[ - \left( \frac{z/H - a}{b} \right)^2 \right] \quad (5)$$

255 where  $a = 0.6$  implies that  $S_{hmax}^d$  occurs at  $z = 0.6H$ ;

256  $b = 0.4$  governs the height of the Gaussian curve.

257 The value of  $a$  and  $b$  can be varied to find a best fit Gaussian curve.  
 258  
 259 New (2017) commented that there is inadequate field data for reliable prediction of horizontal  
 260 soil displacements and these are normally assumed to have similar magnitude to the vertical  
 261 soil displacement. Similarly, GCG (2007) suggested that for ground movements due to shaft  
 262 excavation at the surface  $S_{hmax}^{surface} = S_{vmax}^{surface}$ . In order to examine this assumption, **Figure 9**  
 263 plots vertical and horizontal displacement at the surface from test CR500 and the field  
 264 measurements from New & Bowers (1994). Again, for clarity, only data from one side of test  
 265 CR500 is presented along with field measurements. Whilst the data plotted on Figure 9 are not  
 266 directly comparable (due to significantly large differences in undrained shear strength) it is clear  
 267 from both the centrifuge test results and field measurements that the maximum surface vertical  
 268 displacement is significantly larger than maximum horizontal displacement. Therefore, the  
 269 assumption  $S_{hmax}^{surface} = S_{vmax}^{surface}$  may lead to overestimation of horizontal displacement especially  
 270 at subsurface as  $S_{hz}$  increases with depth  $z$  as shown in **Figure 8**.

271  
 272 Most of the centrifuge test data (with  $d < 0.2H$ ), some of which is presented in **Figure 6**, shows  
 273 values of  $S_{hmax}^d/S_{vmax}^d$  in the range 1 to 1.9. As shown in **Figure 7** and **Equation 4**, maximum  
 274 settlement occurs at surface  $S_{vmax}^d = S_v^{d-surface}$ . With a surface settlement profile estimated by  
 275 **Equation 2**, assuming  $S_{hmax}^d = (1 \text{ to } 1.9)S_v^{d-surface}$  allows a range of horizontal displacements  
 276 at a distance  $d$  at any depth  $z$  to be estimated using **Equation 5** (which would ideally be  
 277 supported by similar case studies). The data from **Figure 9** shows soil displacements in the  
 278 vertical and horizontal directions to be considerably smaller in the field compared with those  
 279 measured in the centrifuge. New and Bowers (1994) reported values of  $S_u$  in London Clay  
 280 varying from 50kPa to 250kPa whereas those in centrifuge test CR500 had an average  $S_u$  of  
 281 approximately 58kPa. Engineers could make a judgement based upon their site soil conditions  
 282 when estimating soil displacements given the information relating to undrained shear strengths  
 283 of clay in the centrifuge tests and the literature contained in this paper. The assumption  $S_{hmax}^d =$   
 284  $(1 \text{ to } 1.9)S_v^{d-surface}$  is examined in a back analysis on field measurements later in this paper.

285

286 COMPARISON BETWEEN CENTRIFUGE TESTS AND SHAFT EXCAVATION IN PRACTICE

287 There are, clearly, significant differences between the reported experiments and the  
288 construction of a shaft in practice. These primarily relate to the method and rate of construction  
289 and the stiffness of the shaft lining. As previously stated, the rate of unloading in the tests was  
290 chosen in order to, as much as possible, replicate an undrained event. The field data utilised  
291 comes from a variety of projects in a variety of soil conditions which may or may not behave in  
292 an undrained way. Nevertheless, good agreement between this field data and the centrifuge  
293 tests has been reported which suggests that the unloading rate had negligible impact on the soil  
294 displacements during shaft excavation.

295 When considering the shaft lining, it could be assumed that the relative hoop stiffness will have  
296 an effect on the magnitude of soil displacements around the shaft excavation (a fact also noted  
297 by Schwamb et al., 2016). The focus of the current work is the pattern, rather than the  
298 magnitude, of subsurface soil displacements induced by shaft excavations. From **Figures 7**  
299 and **8**, it can be seen that despite the (assumed) difference in relative hoop stiffness of the  
300 shafts in the reported case histories compared with the centrifuge tests (arising from the use of  
301 different shaft linings and construction methods), the patterns of subsurface soil displacements  
302 were observed to be similar. This implies that relative hoop stiffness has negligible impact on  
303 the pattern of subsurface soil displacements induced by shaft excavation.

304

305 EXAMPLE APPLICATION OF NEW EQUATIONS

306 **Figure 10** presents a flow chart on how to use **Equations 2, 4 & 5** to predict subsurface vertical  
307 and horizontal displacements. The data set from Wong & Kaiser (1988) is used to demonstrate  
308 their applicability.

309

310 The first stage of the prediction is to generate suitable values of  $n$  and  $\alpha$  for use in **Equation 2**.

311 As previously stated New (2017) acknowledged that these values should be selected with  
312 reference to similar case histories, however in this example there is no such data available. As  
313 such, the original values of New (2017) are adjusted by assessing the ground conditions and  
314 geometry of the shaft reported by Wong & Kaiser (1988). The shaft diameter of Wong & Kaiser  
315 (1988) is approximately four times smaller than the cases reported in New (2017) and the

316 undrained strength of the soils is estimated to be 50% of the strength of London Clay. A  
317 narrower shaft is likely to lead to a narrowing of the surface settlement extent (i.e. a reduction of  
318  $n$ ) and a decrease in settlements generated (i.e. a reduction in  $\alpha$ ). The decrease in soil strength  
319 is likely to lead to an inverse effect (i.e. increase in settlements and extent reflected by  
320 increases in  $n$  and  $\alpha$ ). Using this rationale, estimates of  $n$  and  $\alpha$  are derived from the original  
321 values of  $n = 1.5$  and  $\alpha = 6 \times 10^{-4}$  by doubling these values (to account for soil strength  
322 reduction) and then reducing them by a factor of 4 (to account for reduction in shaft diameter).  
323 This leads to an overall factor of 0.5 and thus values of  $n = 0.75$  and  $\alpha = 3 \times 10^{-4}$ .

324

325 Using these values in **Equation 2** leads to the profile of surface settlement shown in **Figure 11**.  
326 Also plotted are the data from Wong & Kaiser (1988) which shows reasonable agreement with  
327 the profile generated by **Equation 2** whilst acknowledging that the basis for selection of  $n$  and  $\alpha$   
328 values is open to interpretation. A best fit exercise to the measured data was carried out  
329 resulting in very good agreement between the data and **Equation 2**. The values of  $n$  and  $\alpha$   
330 arising from this exercise were 0.85 and  $2.55 \times 10^{-4}$  respectively however, for the purposes of  
331 this discussion, the original estimated values are used.

332

333 Surface settlement at the positions of inclinometer SI#1 ( $d = 0.5m$ ) and extensometer MS#1  
334 ( $d = 1.5m$ ) are determined as  $S_{v-surface}^{SI\#1} = 5.61mm$  and  $S_{v-surface}^{MS\#1} = 4.86mm$  by using distance  
335  $d$  in **Equation 6**. Thus, **Equations 4 & 5** with the determined  $S_{v0}^{MS\#1}$  and  $S_{hmax}^{SI\#1}$  give subsurface  
336 vertical and horizontal displacements which are plotted in **Figures 12a & b** along with the  
337 corresponding field measurements. The limits of the range identified from the centrifuge tests  
338  $S_{hmax}^d/S_v^{d-surface} = (1 \text{ to } 1.9)$  are used to generate the two curves in **Figure 12b**.

339

340 The predicted vertical displacement with depth is marginally smaller than the measured values.  
341 Nevertheless, the predicted vertical displacement with depth is very similar with the field  
342 measurement in terms of magnitude and shape.

343

344 For subsurface horizontal displacement, the assumption  $S_{hmax}^d = S_v^{d-surface}$  provided a very  
345 good fit with the field measurement whereas  $S_{hmax}^d = 1.9S_v^{d-surface}$  overestimated the magnitude  
346 of soil deformations. More field data are needed to assess whether  $S_{hmax}^d = S(1 \text{ to } 1.9)_v^{d-surface}$   
347 and caution should be exercised when applying this relationship.

348

#### 349 CONCLUSION

350 The results of centrifuge tests carried out in this research show good agreement with field data  
351 from various shaft projects which provides a clearer insight into subsurface soil displacements  
352 due to shaft excavation. Based on experimental evidence and field measurements, two novel  
353 empirical equations have been suggested to describe unique distributions of soil movements  
354 with depth regardless of soil conditions, construction techniques and shaft dimensions. A flow  
355 chart on how to use these equations to predict soil movements in any direction at any point is  
356 provided for practical use.

357

#### 358 ACKNOWLEDGEMENT

359 The authors gratefully acknowledge the support of the Leverhulme Trust grant no. RPG-2013-  
360 85 and support from colleagues from Research Centre for Multi-scale Geotechnical  
361 Engineering, at City, University of London.

362

#### 363 REFERENCES

- 364 Divall, S. and Goodey, R. J. (2016). An apparatus for centrifuge modelling of a shaft  
365 construction in clay. In Eurofuge2016, 3<sup>rd</sup> European Conf. on Physical Modelling in  
366 Geotechnics, Nantes, France.
- 367 Faustin, N.E (2017). Performance of circular shafts and ground behaviour during construction.  
368 PhD thesis, University of Cambridge.
- 369 GCG. (2007) Settlement Estimation Procedure: Box Excavations & Shafts. B London, Crossrail.  
370 Report number: 1D0101-G0G00-01004.
- 371 Grant, R.J. (1998). Movements around a tunnel in two-layer ground. PhD thesis, City University  
372 London.



373 Le, B.T., Nadimi, S., Goodey, R.J. and Taylor, R.N. (2016). System to measure three  
374 dimensional movements in physical models. *Géotechnique Letters*, 6(4), pp.256-262.

375 Mayne, P.W. and Kulhawy, F.H. (1982). Ko- OCR Relationships in Soil. *Journal of the Soil*  
376 *Mechanics and Foundations Division*, 108(6), pp.851-872.

377 McNamara, A., Roberts, T., Morrison, P. and Holmes, G. (2008). Construction of a deep shaft  
378 for Crossrail. In Proc. Instn Civ. Engrs Geotech. Engng, volume 161, pages 299–309.

379 New, B. (2017). Settlements due to shaft construction. In *Tunnels and tunnelling international*,  
380 September 2017, pp. 16-17.

381 New, B. and Bowers, K. (1994). Ground movement model validation at the Heathrow Express  
382 trial tunnel. In Tunnelling '94 Proc. 7th Int. Symp. IMM and BTS, pages 301–329, London.  
383 Chapman and Hall.

384 Parry, R.H.G. (1970). Overconsolidation in soft clay deposits. *Géotechnique*, 20(4), pp.442-446.

385 Schwamb, T. (2014). Performance Monitoring and Numerical Modelling of a Deep Circular  
386 Excavation. Phd thesis, University of Cambridge.

387 Schwamb, T., Soga, K., Elshafie, M. Z. E. B., and Mair, R. J. (2016). Considerations for  
388 monitoring of deep circular excavations. Proc. Instn Civ. Engrs Geotech. Engng, 169(6):477–  
389 493.

390 Stanier, S.A. Blaber, J., Take, W.A. & White, D.J. (2015). Improved image based deformation  
391 measurement for geotechnical applications. *Canadian Geotechnical Journal*.

392 Taylor, R.N. (ed.) (1995). *Geotechnical Centrifuge Technology*. Blackie Academic and  
393 Professional, Glasgow.

394 Wong, R. C. K. R. and Kaiser, P. P. K. (1988). Behaviour of vertical shafts: reevaluation of  
395 model test results and evaluation of field measurements. *Canadian Geotechnical Journal*,  
396 25(2):338–352.

397

398

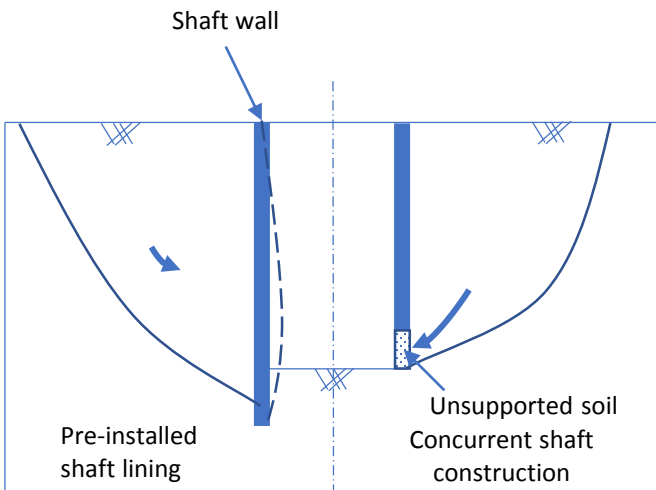
399	LIST OF FIGURES
400	Figure 1: Sources of ground movements due to shaft construction (after Faustin, 2017).
401	Figure 2: Surface settlement data from 13 shafts (after New, 2017).
402	Figure 3: Schematic of centrifuge test apparatus.
403	Figure 4: Profiles of $K_0$ and OCR with depth in centrifuge models.
404	Figure 5. Soil deformations in test CR500 after all fluid was drained out.
405	Figure 6: Typical subsurface soil displacements in test CR500.
406	Figure 7: Subsurface vertical movements.
407	Figure 8: Subsurface horizontal movements.
408	Figure 9: Displacements at surface in centrifuge test and New & Bowers (1994).
409	Figure 10: Suggested flow chart on the usage of the proposed equations.
410	Figure 11: Comparison on Surface settlement in Wong & Kaiser (1988) and back analysis using
411	Equation 2.
412	Figure 12: Comparison on subsurface soil displacements in Wong & Kaiser (1988) and back
413	analysis using Equations 4 & 5.
414	

No	Reference	Location	Construction method	Ground conditions	Shaft geometry		Available ground movements data
					D (m)	H (m)	
1	Wong & Kaiser (1988)	Edmonton, Canada	Concurrent shaft lining Corrugated and Flanged steel plates	Sand & clay (6.5m) Glacial matrix (13m) Clay shale	2.4 to 3.2	20	Surface: Sv Subsurface Sh, Sv
2	Schwamb et al. (2016)	London, UK	Pre-installed shaft lining Diaphragm wall	London basin deposits	30	73	Subsurface Sh, Sv
3	McNamara et al. (2008)	London, UK	Concurrent shaft lining Pre-cast segments	London clay (30m) Lambeth Group (18m)	8.2	37.5	Subsurface Sh
4	New & Bower (1994)	London, UK	Concurrent shaft lining Pre-cast segments (16m) SCL (10m)	Superficial deposits (3.5m) London Clay	10.65	26	Surface Sh, Sv
5	This study	City, University of London	Pre-installed shaft lining	Speswhite kaolin	8*	20*	Surface Sv, Sh Subsurface Sv, Sh

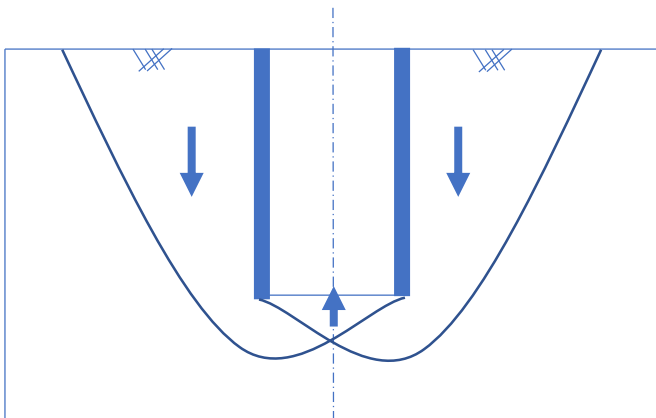
\* dimension in equivalent prototype.

Table 1. Case histories used in this paper.

Figure 1



a) Ground movement caused by radial unloading



b) Ground movement caused by vertical unloading

Fig. 1: Sources of ground movements due to shaft construction (after Faustin, 2017).

Figure 2

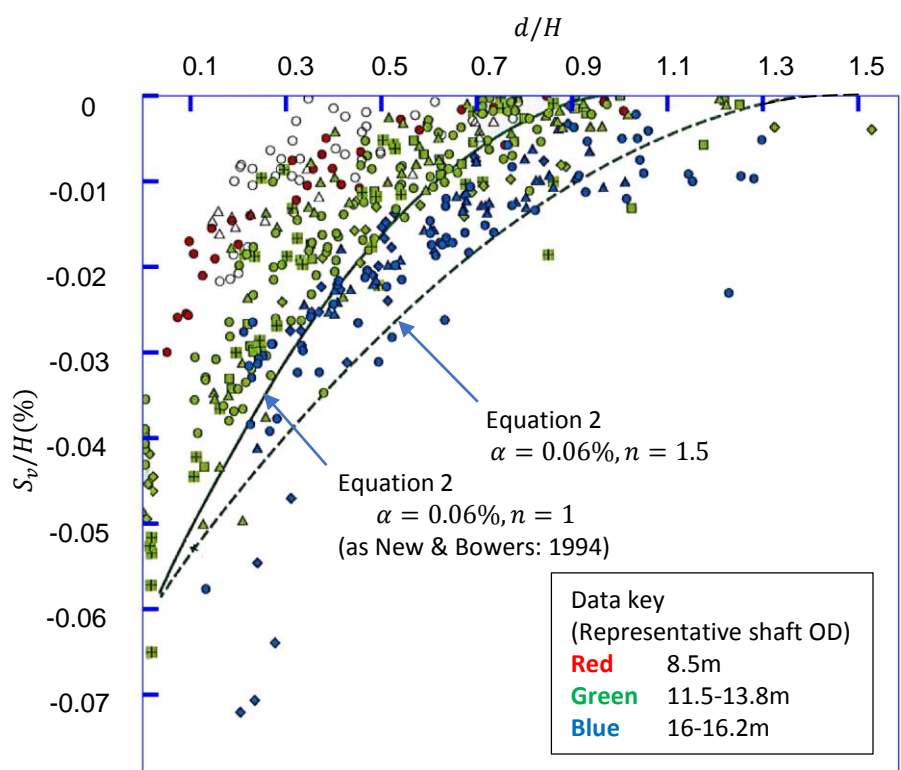


Fig. 2: Surface settlement data from 13 shafts (after New, 2017).



Figure 4

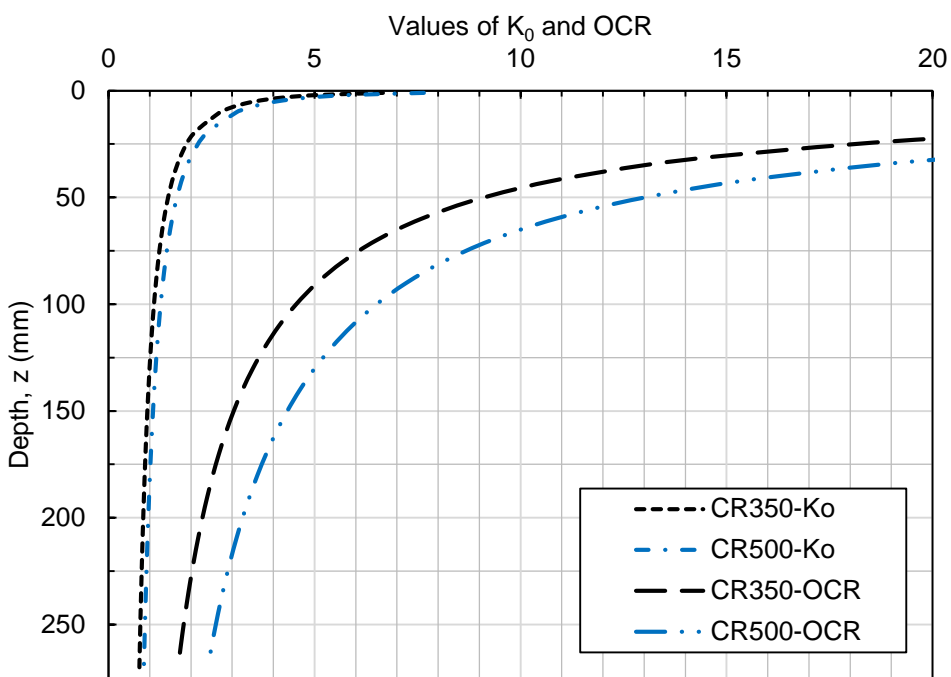
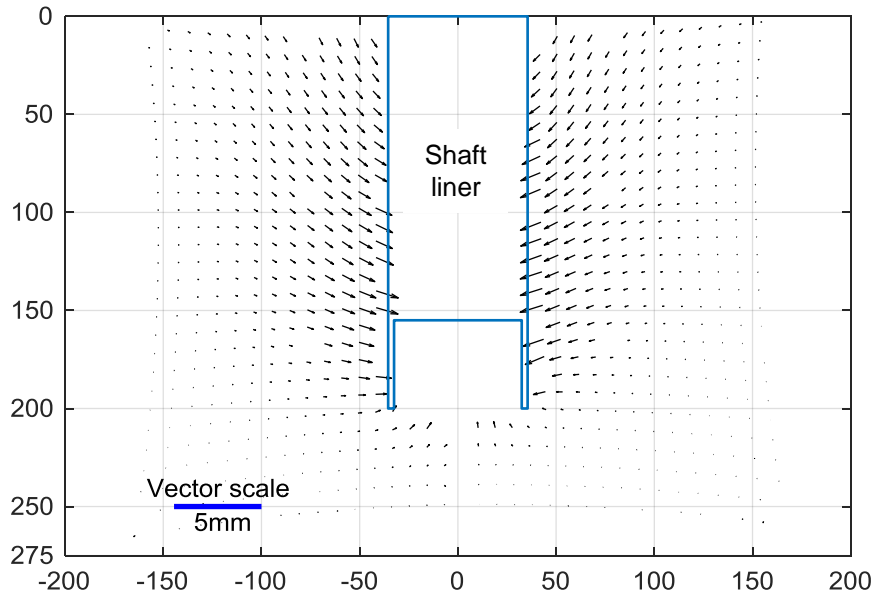
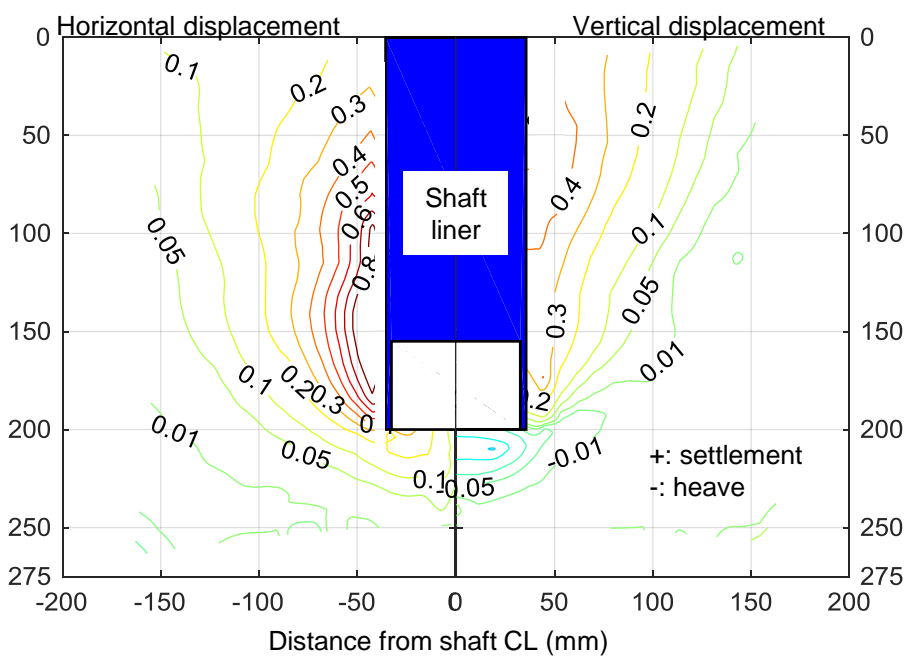


Fig. 4: Profiles of  $K_0$  and OCR with depth in centrifuge models.

Figure 5



a) Soil displacement field



b) Horizontal and vertical displacement contours

Fig. 5. Soil deformations in test CR500 after all fluid was drained out.



Figure 6

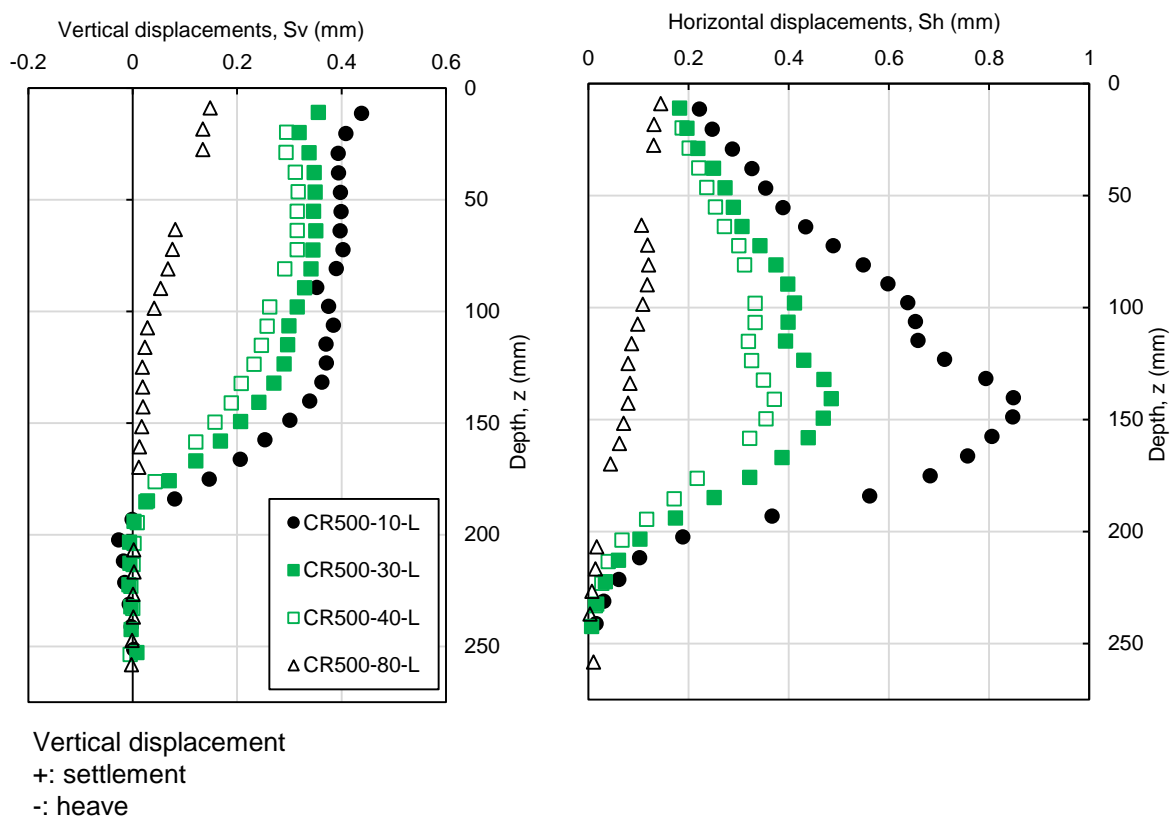


Fig. 6: Typical subsurface soil displacements in test CR500.

Figure 7

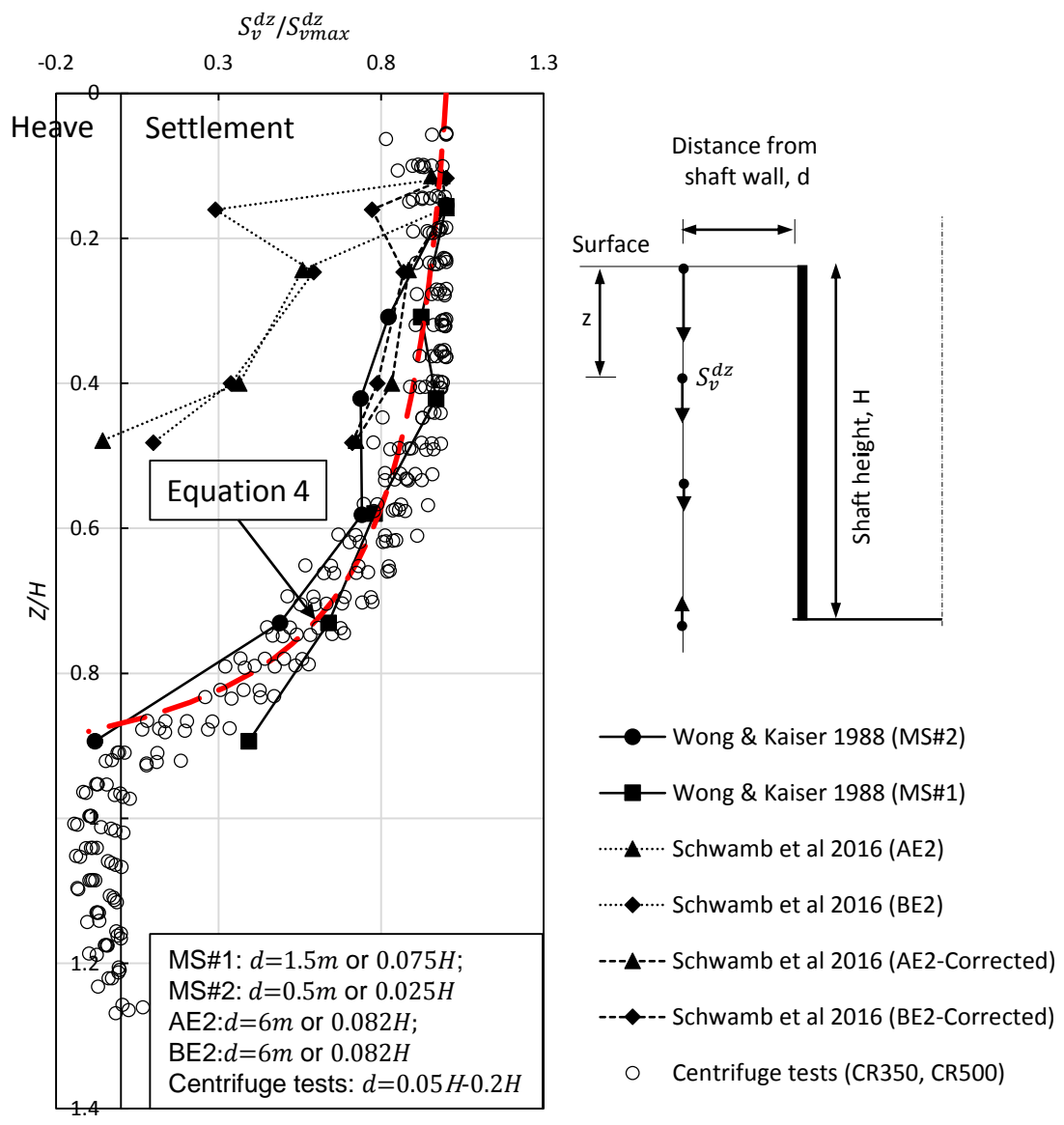


Fig. 7: Subsurface vertical movements.

Figure 8

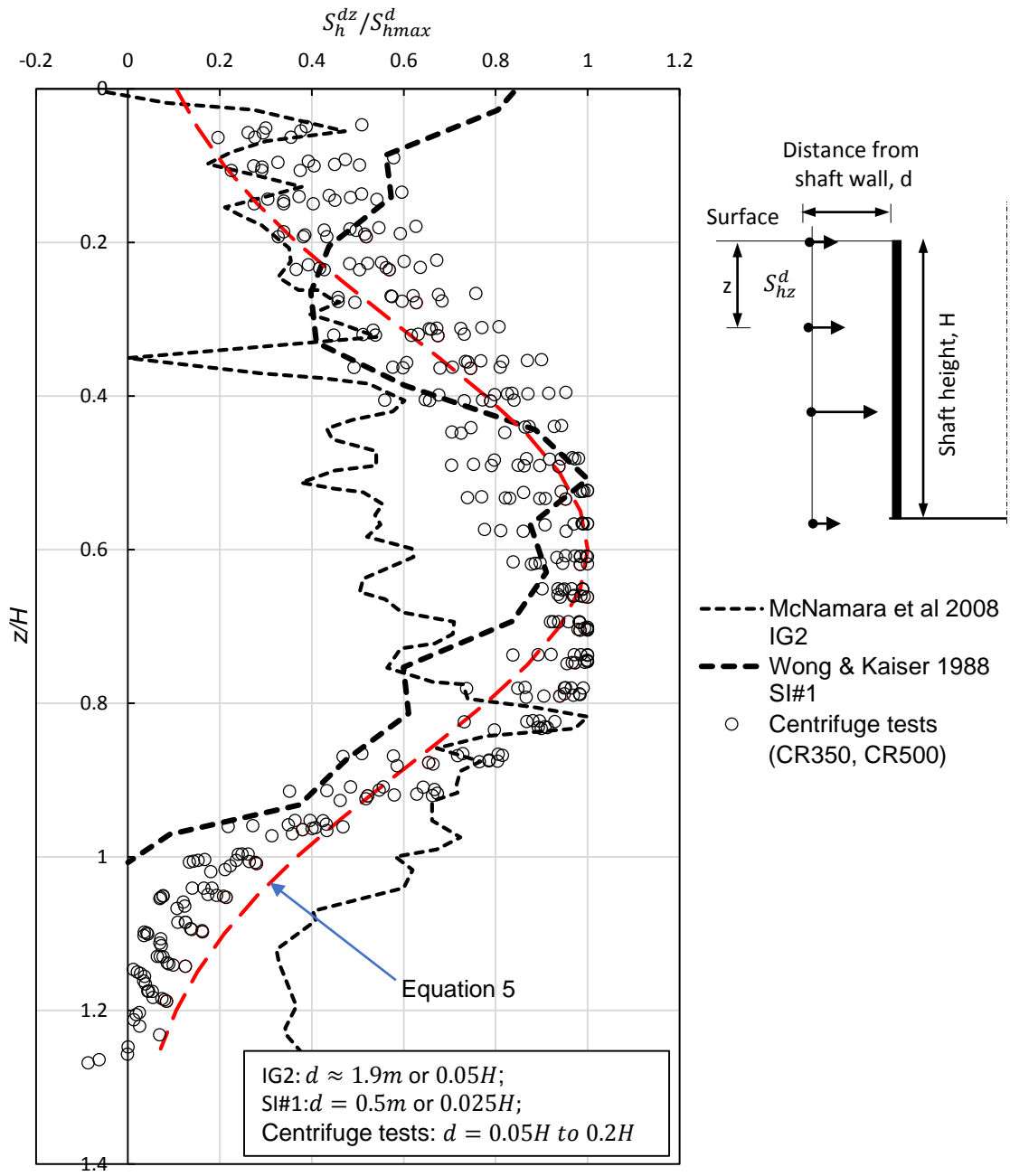


Fig. 8: Subsurface horizontal movements.

Figure 9

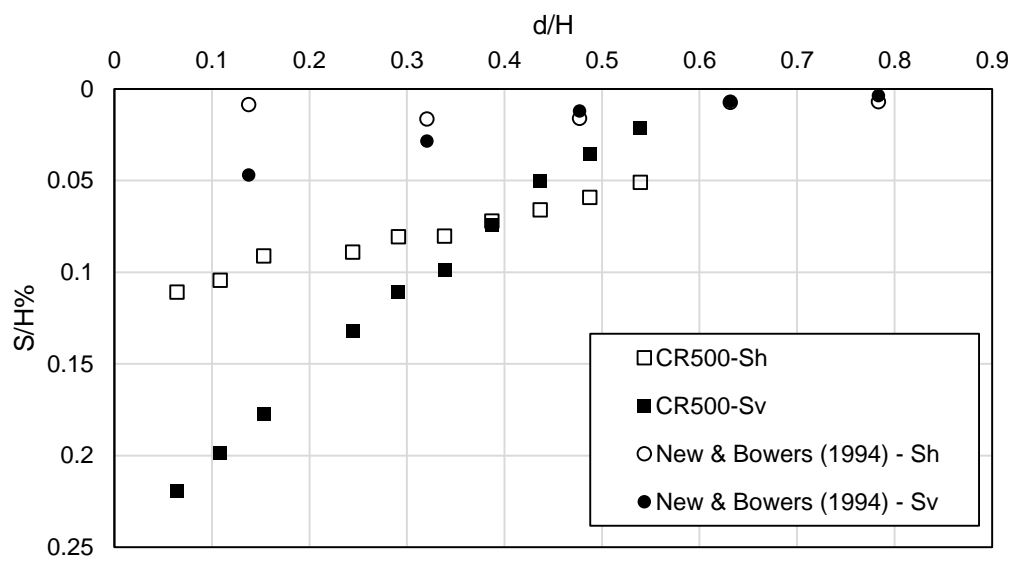


Fig. 9: Displacements at surface in centrifuge test and New & Bowers (1994).

Figure 10

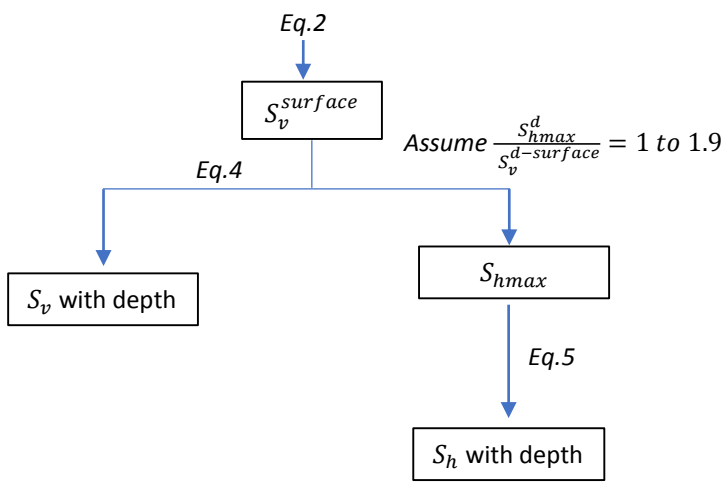


Fig. 10: Suggested flow chart on the usage of the proposed equations.

Figure 11

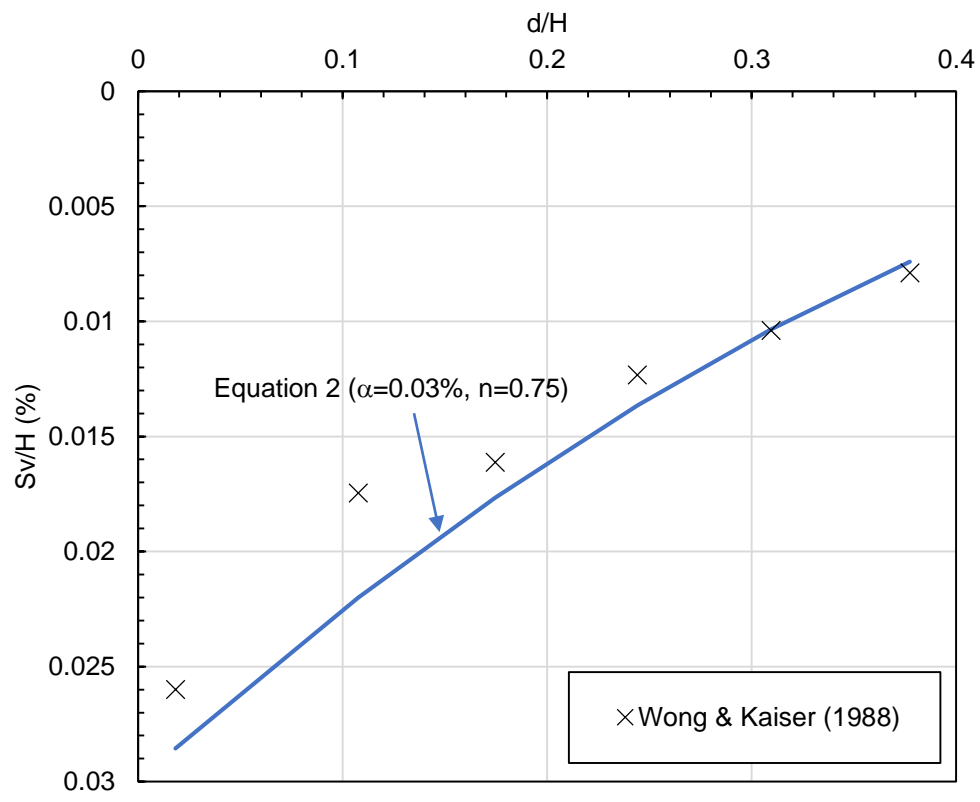


Fig. 11: Comparison on Surface settlement in Wong & Kaiser (1988) and back analysis using Equation 2.

Figure 12

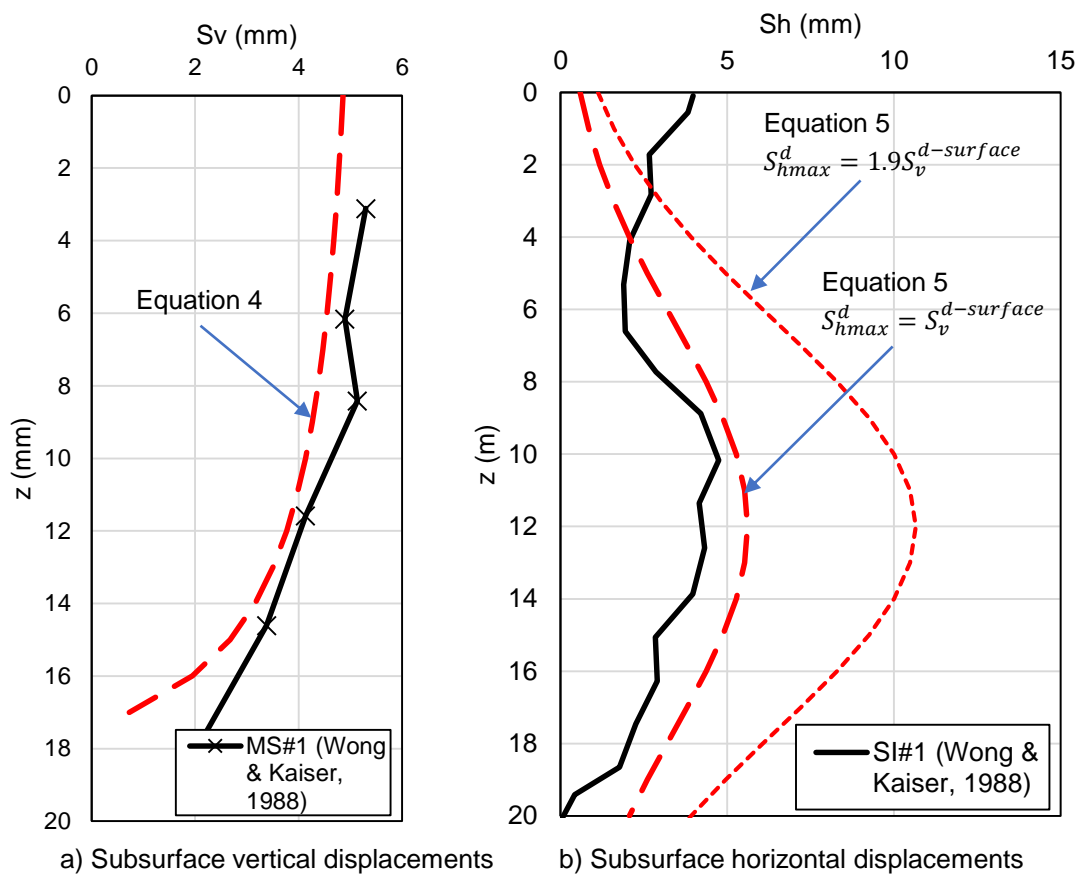


Fig. 12: Comparison on subsurface soil displacements in Wong & Kaiser (1988) and back analysis using Equations 4 & 5.